Toxicology in Vitro 108 (2025) 106100

Contents lists available at ScienceDirect

Toxicology in Vitro

journal homepage: www.elsevier.com/locate/toxinvit

CiPA-qualified human iPSC-derived cardiomyocytes: A new frontier in toxicity testing by evaluating drug-induced arrhythmias☆

Vijay Bhaskar Reddy Konala [a], Rutuja Kuhikar [a], Shruti More [a], Matthias Gossmann [b], Bettina Lickiss [b], Peter Linder [b], Jaganmay Sarkar [a], Paresh Bhanushali [a], Amit Khanna [a,*]

[a] Department of Integrated Drug Discovery and Development, C113, Yashraj Biotechnology Ltd, TTC Industrial Area MIDC, Pawnae, Navi Mumbai 400705, Maharastra, India
[b] innoVitro GmbH, Artilleriestr 2, 52428 Jülich, Germany

ARTICLE INFO

Editor: P Jennings

Keywords:
CiPA
hiPSC-CMs
YBLiCardio
Cardiotoxicity
Drug-induced arrhythmias
Electrophysiology
Preclinical assays
Acute toxicity
Chronic toxicity

ABSTRACT

Drug-induced arrhythmias remain a significant challenge in drug development, often leading to serious cardiovascular complications and the withdrawal of approved drugs from the market. The Comprehensive in vitro Proarrhythmia Assay (CiPA) initiative aims to enhance cardiac safety assessment by leveraging human-induced pluripotent stem cell-derived cardiomyocytes (hiPSC-CMs). In this study, we evaluated the effects of 28 drugs on a well-characterized hiPSC-CMs (YBLiCardio, Yashraj Biotechnology Ltd., Mumbai, India) using Electric Field Potential (EFP) measurements. The CardioExcyte 96 system recorded extracellular signals from 96 wells, functioning similarly to microelectrode arrays. Each drug was tested at four concentrations, and the effects were analyzed based on dynamic changes in beat patterns, with QT prolongation assessed by measuring the interval between the sodium spike and T-wave. Our results demonstrated that YBLiCardio cells responded to all drugs in line with the findings from the HESI CiPA study. Notably, droperidol (173 %) and domperidone (182 %), originally classified as intermediate-risk compounds, were identified as high-risk in our model, consistent with previous findings by Nguyen et al. (2017). Additionally, YBLiCardio showed enhanced predictive accuracy for chlorpromazine. These findings highlight the potential of hiPSC-CMs for proarrhythmia risk assessment within the CiPA framework, complementing ion channel data and in silico modeling approaches. Overall, YBLiCardio provides a robust and physiologically relevant platform for predicting cardiotoxicity, supporting safer and more efficient pre-clinical drug discovery & development.

1. Introduction

The development of new pharmaceuticals is often hindered by the risk of drug-induced arrhythmias, which can lead to severe cardiovascular complications and the eventual withdrawal of drugs from the market. Traditional preclinical models - primarily based on animal studies or isolated cardiac tissues- frequently fail to accurately predict human cardiac responses, thereby creating a critical gap in cardiotoxicity and safety assessment. This gap contributes to high attrition rates in drug development, substantial financial costs, and increased risk to patients in need of effective therapies (Seyhan, 2019).

Multiple studies have documented the withdrawal of marketed drugs due to unforeseen cardiotoxicity. For instance, an analysis of 121 drugs withdrawn between 1960 and 1999 found that 8.7 % were removed due to unexpected cardiotoxic effects (Fung et al., 2001), similarly, 14 % of drugs withdrawn between 1953 and 2013 were associated with unanticipated n cardiovascular side effects (Onakpoya et al., 2016). More recently, 27 out of 78 drugs with known cardiovascular risks were withdrawn for overt cardiotoxicity (Mamoshina et al., 2021).

Examples include dronedarone, initially approved for treating atrial fibrillation, but later shown to increase mortality in patients with pre-existing heart failure (Singh et al., 2007; Køber et al., 2008). Likewise, the anthracycline class of anticancer drugs, despite their well-known link to cardiac dysfunction- remains widely used (Di Marco et al., 1964; Tan et al., 1967). Other drug classes, such as anti-diabetics (Lee et al., 2022), fluoroquinolone antibiotics (Frothingham, 2001), and selective serotonin reuptake inhibitors (Funk and Bostwick, 2013), have also shown post-market proarrhythmic effects.

☆ This article is part of a Special issue entitled: 'ESTIV 2024' published in Toxicology in Vitro.

* Corresponding author.
E-mail address: amit.khanna@yashraj.com (A. Khanna).

https://doi.org/10.1016/j.tiv.2025.106100
Received 12 February 2025; Received in revised form 19 May 2025; Accepted 3 June 2025
Available online 5 June 2025
0887-2333/© 2025 Elsevier Ltd. All rights are reserved, including those for text and data mining, AI training, and similar technologies.

To mitigate such risks, regulatory agencies have mandated testing for hERG potassium channel inhibition and QT interval prolongation on electrocardiograms (FDA, 2005a, 2005b). While these tests have successfully identified drugs that induce torsades de pointes (TdP), these assessments can lead to the premature rejection of therapeutically valuable compounds—especially those with multichannel effects (Stockbridge et al., 2013). For example, drugs like verapamil (a dual hERG and L-type calcium blocker) and ranolazine (which blocks the late sodium current) may yield misleading results when evaluated solely for hERG inhibition (Johannesen et al., 2014). These limitations have prompted the development of the Comprehensive in Vitro Proarrhythmia Assay (CiPA), a more integrated and mechanistically informed approach to assess proarrhythmic risk (Colatsky et al., 2016; Fermini et al., 2016; Sager et al., 2014; Blinova et al., 2017).

Human-induced pluripotent stem cell-derived cardiomyocytes (hiPSC-CMs) have emerged as a promising solution to overcome the shortcomings of traditional models. By reprogramming somatic cells into pluripotent cells and differentiating them into cardiomyocytes, hiPSC-CMs offer a physiologically and genetically relevant human platform for evaluating drug-induced cardiotoxicity. The CiPA initiative has recognized their value by incorporating hiPSC-CMs into its multi-tiered testing strategy, providing a more accurate and comprehensive framework for arrhythmia risk assessment.

This study is particularly significant in light of the FDA Modernization Act 2.0 (2022), which supports the use of advanced non-animal methodologies in drug development and regulatory safety testing. The act reinforces the importance of developing and validating human-relevant platforms such as hiPSC-CMs to accelerate safer drug discovery and reduce reliance on animal models. This manuscript highlights the characterization and application of YBLiCardio hiPSC-CMs in toxicity testing, underscoring their transformative potential in next-generation cardiac safety assessment.

2. Materials and methods

2.1. hiPSC culture

An in-house-derived human induced pluripotent stem cell (hiPSC) line (YBLi001A) (Chitrangi et al., 2023) was used for all differentiation experiments. Cells were cultured on Matrigel-coated six-well plates using mTeSR™ Plus medium (STEMCELL Technologies) under feeder-free conditions, as previously described (Konala et al., 2020). Routine passaging was performed when cells reached ~80 % confluency, and cells were seeded at a density of 2×10^5 cells per well in a 6 well plate for maintenance and expansion. Refer to the Resource Table 1 for details on the media, reagents, and plasticware used in the differentiation experiments.

Table 1
List of Media, reagents and plasticware used for generating YBLiCardio cells. (For interpretation of the references to colour in this figure legend, the reader is referred to the web version of this article.)

REAGENT or RESOURCE	SOURCE	IDENTIFIER
hiPSCs	YBL	Cat# YBLi001A
Matrigel hESC-Qualified Matrix	Corning	Cat# 354277
mTesR Plus media	StemCell Technologies	Cat# 100–0276
StemDiff Cardiomyocyte Differentiation and Maintenance Kit	StemCell Technologies	Cat# 5010
STEMdiff Cardiomyocyte Dissociation Kit	StemCell Technologies	Cat# 5020
STEMdiff Cardiomyocyte Freezing media	StemCell Technologies	Cat# 5030
STEMdiff Cardiomyocyte Maintenance media	StemCell Technologies	Cat# 5020
ReLeSR	StemCell Technologies	Cat# 100–0483
Revita	ThermoFisher	Cat# A2644501
DPBS	ThermoFisher	Cat# 14040133
DMEM/F12	ThermoFisher	Cat# A4192001
T-75 flasks	ThermoFisher	Cat# 156499
6 well plates	ThermoFisher	Cat# 140685
24 well plate	ThermoFisher	Cat# 142475
1 mL filter tips	ThermoFisher	Cat# AM12665TS
1.5 mL eppendorf tubes	ThermoFisher	Cat# AM12400
200uL filter tips	ThermoFisher	Cat# 94052320
10uL filter tips	ThermoFisher	Cat# 94052100
Chamber slides	ThermoFisher	Cat# 154534
0.5 mL Ependroff tubes	ThermoFisher	Cat# AM12350
10 mL serological pipettes	ThermoFisher	Cat# 170356 N
5 mL serological pipettes	ThermoFisher	Cat# 170366 N
15 mL conical tubes	ThermoFisher	Cat# 339650
50 mL conical tubes	ThermoFisher	Cat# 339652
Cryovials	Nunc	Cat# 377267
Trypan Blue	ThermoFisher	Cat# 15250061

2.2. In vitro generation of YBLiCardio from induced pluripotent stem cells (iPSCs)

Human iPSCs were maintained on hESC-qualified Matrigel in mTeSR1 medium (STEMCELL Technologies) under standard feeder-free conditions. For cardiomyocyte differentiation, a monolayer-based protocol was followed using the STEMdiff™ Cardiomyocyte Differentiation Kit, according to the manufacturer's instructions. Spontaneously contracting cardiomyocytes were typically observed by day 8 of differentiation, with contractile function maintained through to cryopreservation and restored within 3–4 days post-thaw (Fig. 1A, Supplementary Videos 1).

2.3. Cryopreservation and thawing for characterization, acute and chronic toxicity assays

YBLiCardio cells were cryopreserved using STEMdiff™ Cardiomyocyte Freezing Medium (STEMCELL Technologies) following the manufacturer's instructions. Briefly, cells were washed twice with Dulbecco's Phosphate-Buffered Saline (DPBS; Thermo Fisher Scientific) and incubated with STEMdiff™ Cardiomyocyte Dissociation Reagent (STEMCELL Technologies) for 20–30 min at 37 °C to facilitate single-cell dissociation. The resulting suspension was collected and centrifuged at 300 ×*g* for 5 min. The cell pellet was then resuspended in pre-chilled STEMdiff™ Cardiomyocyte Freezing Medium (STEMCELL Technologies), and 1.2×10^6 cells were aliquoted per cryovial. Cryovials were transferred to a controlled-rate freezing container (Mr. Frosty, Thermo Fisher Scientific) and stored at −80 °C for 24 h before being transferred to liquid nitrogen for long-term storage, as per established protocols for cardiomyocyte cryopreservation (Lundy et al., 2013).

For recovery, cells were thawed after 48 h using STEMdiff™ Cardiomyocyte Support Medium (STEMCELL Technologies). Vials were rapidly thawed in a 37 °C water bath and transferred dropwise into pre-warmed Support Medium. Cells were then plated onto Matrigel-coated (Corning, NY, USA) tissue culture dishes and maintained under standard conditions (37 °C, 5 % CO_2) for four days to allow recovery of morphology and spontaneous contractility. Once the cardiomyocytes exhibited typical polygonal morphology and synchronous beating—typically by four days post-thaw—they were subjected to downstream assays for molecular profiling, protein expression, and gene expression analyses, as well as acute and chronic toxicity assessments, in accordance with established protocols (Ronaldson-Bouchard et al., 2019; Lundy et al., 2013) at Day 20.

2.4. Quantitative RT-PCR

Total RNA was extracted using RNeasy Mini Kit (Qiagen, 74,104) as per the manufacturer's protocol. 1 μg of total RNA was converted to cDNA using a iScript™ cDNA Synthesis Kit (#1708891, Biorad, USA)

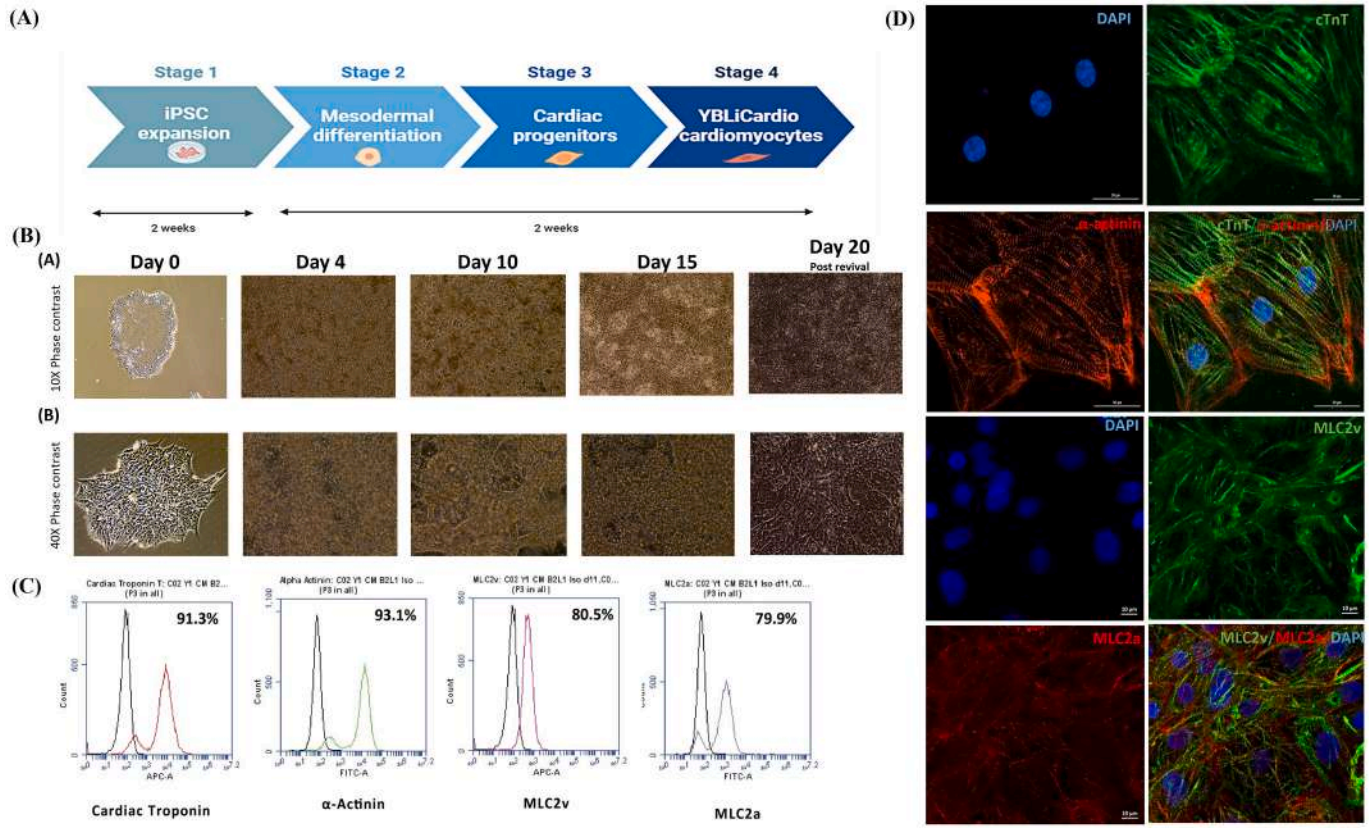

Fig. 1. A) Schematic representation of the differentiation protocol. hiPSC expansion is followed by the subsequent differentiation from mesodermal lineage to progenitor stage followed by the generation of functional cardiomyocytes. B) Phase contrast images of differentiation procured on day 0, day 4, day 10, day 15 and day 20 depicting the morphological changes observed in hiPSCs (Day 0) up to the generation of functional adult cardiomyocytes (Day 20). C) Flowcytometric analysis of cardiac specific markers such as cardiac troponin, alpha actinin, MLC2v and MLC2a. The expression of cardiac troponin (91.3 %), alpha actinin (93.1 %), MLC2v (80.5 %) and MLC2a (79.9 %) validates the differentiation of hiPSCs to cardiomyocytes. D) Immunofluorescence images of YBLiCardio stained for cardiac troponin (CTNT), alpha actinin (α actinin), MLC2v and MLC2a. Scale bar represents 10 μm.

according to the manufacturer's protocols. Quantitative PCR was performed using HOT FIREPol EvaGreen qPCR Mix Plus (ROX) Kit (Solis Biodyne 08–24-00001). Gene expression was normalized to 18S rRNA, and relative mRNA levels were calculated using Ct values. All reactions were run in triplicate. Primer sequences are provided in Table 2.

2.5. Flow cytometry

Cells were fixed and permeabilized using Intracellular Fixation & Permeabilization Buffer kit (eBioscience, 88–8824-00). Cells were then incubated with specific flurochrome tagged antibodies for 45 min in the dark at 4 °C. The stained cells were washed, resuspended in 1XPBS, and acquired on BD Accuri™ C6 plus Flow Cytometer (BD Biosciences). Isotype-matched controls were included. Data were processed using BD Accuri™ software. Antibody details are listed in Table 3.

2.6. Immunofluorescence

Cells were cultured on 8 well chamber slides, fixed with 4 % paraformaldehyde for 10 min, and permeabilized with 0.5 % Triton X-100 for 5 min at Room temperature. Blocking was performed with 5 % bovine serum albumin for 1 h, followed by overnight incubation with primary antibodies at 4 °C. The next day, cells were washed and incubated with secondary antibodies at room temperature for 1 h. After washing, nuclei were counterstained with DAPI (Invitrogen). Immunofluorescence images were acquired using a Zeiss LSM780 confocal laser scanning microscope. The details of the antibodies used are mentioned in Table 4.

2.7. RNA sequencing

To determine the gene expression profiling of hiPSC-derived YBLiCardio with human heart RNA and parental hiPSCs, we have performed RNA sequencing analysis. Samples were collected on Days 0, 6, and 15 to examine the maturation trajectory of cardiomyocyte differentiation. Additionally, Day 30 samples generated by thawing Day 15 cardiomyocytes and culturing them for a further 15 days were included to represent a more mature cardiomyocyte stage.

Table 2
List of primers used for real time qPCR.

Target gene	Make	Forward primer sequence	Reverse primer sequence	Product length
CTNT2	Sigma	TTCACCAAAGATCTGCTCCTCGCT	TTATTACTGGTGTGGAGTGGGTGTGG	166
MYL2	Sigma	TGTCCCTACCTTGTCTGTTAGCCA	ATTGGAACATGGCCTCTGGATGGA	135
MYH7	Sigma	TCGTGCCTGATGACAAACAGGAGT	ATACTCGGTCTCGGCAGTGACTTT	83
MESP1	Sigma	AGCCCAAGTGACAAGGGACAACT	AAGGAACCACTTCGAAGGTGCTGA	82

Table 3
List of conjugated antibodies used for flowcytometry Staining.

Name of antibody	Catalogue number	Make	Host	Dilutions
Cardiac Troponin T Antibody, anti-human/mouse/rat, APC, REAfinity#, Clone REA400	130–120-403	Miltenyi Biotec	Human	1:50
á-Actinin (Sarcomeric) Antibody, anti-human/mouse/rat, FITC, REAfinity#, Clone REA402	130–119-766	Miltenyi Biotec	Human	1:50
MLC2v Antibody, anti-human/mouse/rat, APC, REAfinity#, Clone REA401	130–123-847	Miltenyi Biotec	Human	1:50
MLC2a Antibody, anti-human/mouse/rat, FITC, REAfinity#, Clone REA398	130–106-141	Miltenyi Biotec	Human	1:10
REA Control Antibody (I), human IgG1, APC, REAfinity#, Clone REA293	130–120-709	Miltenyi Biotec	Human	1:50
REA Control Antibody (I), human IgG1, FITC, REAfinity#, Clone REA293	130–118-354	Miltenyi Biotec	Human	1:50

Table 4
List of unconjugated primary and conjugated secondary antibodies used for Immunofluorescence Staining.

Name of antibody	Catalogue number	Make	Host	Dilutions
Cardiac Troponin T Recombinant Rabbit Monoclonal Antibody (17H8L13)	701,620	Invitrogen	Rabbit	1:100
Monoclonal Anti-α-Actinin (Sarcomeric) antibody produced in mouse	A7811-100UL	Sigma	Mouse	1:100
Anti-Myosin Light Chain 2 antibody	ab79935	abcam	Rabbit	1:100
Anti-MYL7 antibody	ab68086	abcam	Mouse	1:100
Goat Anti-Rabbit IgG H&L (Alexa Fluor® 488) preadsorbed	ab150081	abcam	Goat	1:2000
Goat Anti-Mouse IgG H&L 647	ab150115	abcam	Goat	1:2000

2.8. RNA extraction

Total RNA was extracted using the Qiagen RNeasy Mini Kit according to the manufacturer's instructions with minor modifications. Briefly, cell pellets were lysed in TRIzol reagent supplemented with β-mercaptoethanol and homogenized using a Tissue Lyser. After phase separation by centrifugation, the aqueous phase was mixed with 70 % ethanol and applied to RNeasy columns. Columns were washed with RW1 and RPE buffers, followed by RNA elution in 50 μL of elution buffer. Extracted RNA was quantified using Nanodrop and Qubit fluorometer, and RNA integrity was assessed with the Agilent 4200 TapeStation.

2.9. Library preparation, and quality control

One microgram of total RNA was depleted of rRNA using the NEBNext rRNA Depletion Kit (Human, Mouse, Rat, Cat.no: E7405) following the manufacturer's instructions. rRNA-depleted RNA was used to prepare directional RNA-seq libraries with the NEBNext Ultra II Directional RNA Library Prep Kit (Illumina, Cat,no: E7760L). Library preparation included RNA fragmentation, cDNA synthesis, adapter ligation, and PCR enrichment. Libraries were quantified using Qubit and assessed for fragment size distribution on an Agilent 4200 TapeStation. Quality-checked libraries were sequenced on an Illumina NovaSeq platform using 150 bp paired-end chemistry.

2.10. Reads filtering, trimming and mapping

The quality of the reads was assessed using FastQC v0.11.9 (Andrews, 2010) prior to downstream analysis. Raw reads were processed with fastp v0.23.2 (Chen, 2023) to remove adapters, low-quality reads ($q < 30$), and reads with lengths less than 36 nucleotides after adapter trimming. Quality improvement was verified using FastQC before proceeding further. Adapter-free reads were filtered for ribosomal RNA (rRNA) sequences using SortMeRNA v4.3.6 (Kopylova et al., 2012) against eight different rRNA databases. The rRNA-filtered reads were mapped to the reference genome using HISAT2 v2.2.1 (Kim et al., 2019). Read quantification was performed with feature Counts v2.0.1 (Liao et al., 2014). For both mapping and quantification steps, a prebuilt human genome index and GTF file (*Homo sapiens* GRCh38) from ENSEMBL were utilized.

2.11. Differential expression analysis

Raw counts files were processed to remove transcripts with low read counts (< 10 counts in all samples). The filtered read counts were used as input for DESeq2 analysis in R (Love et al., 2014). To assess sample-to-sample distances, a heatmap of the distance matrix was generated, providing an overview of the similarities and dissimilarities between samples. Principal Component Analysis (PCA) was conducted to visualize the clustering of samples. Significant DEGs were filtered based on a false discovery rate (FDR) cutoff of $\leq$0.05 and a minimum expression fold change (FC) of $\geq$2, and the results were inspected with a volcano plot (using the enhanced volcano plot r package). The relative expression levels of the top 100 most variably expressed genes were visualized using heat map package. Separate heat maps were created for each comparison based on top 25 up regulated and top 25 down regulated genes which are significantly expressed. Heatmap was also created for specific genes of interest. Each gene's values were centered across samples to provide more meaningful insights.

2.12. Compound assay conduction for Acute and Chronic effects

The FLEXcyte 96 device was operated in a humidified cell culture incubator at 37 °C and 5 % CO2. Four hours prior to the experiment, the medium in all wells was changed. Test compound dilution series were prepared in a 1 mL deep-well plate as 4× concentrated solutions in Maintenance Medium and equilibrated in a cell culture incubator for 2 h. Baseline measurements were conducted at 5-min intervals, starting 15 min before compound addition. The last measurement before compound addition was used as the reference measurement. For test compound addition, the plate was removed from the device and transferred to a laminar flow hood. From each well, 50 μL of the assay buffer was aspirated and the same volume of compound-containing assay buffer was added using a 12-channel electronic pipette. Subsequently, the plate was reinserted into the FLEXcyte 96 device, and the compound measurement was initiated. Acute measurements were conducted in intervals of 5-min intervals over a 20-min period. Chronic measurements were conducted at 1 h, 24 h, 48 h, and 72 h after compound addition. Refer to Table 5 for the list of acute and chronic compounds. We evaluated the contractile profiles of iPSC-derived cardiomyocytes treated with tool compounds at four concentrations. The primary readouts included amplitude, beating rate, beat duration, area under the curve (AUC), and the slopes of contraction and relaxation (Supplementary Fig. 6).

2.13. Test compound selection and preparation for CiPA study

The 28 CiPA test compounds and the experimental procedure were followed exactly as described in the consortium study (Blinova et al.,

Table 5
List of compounds used for measuring acute and chronic toxicity.

Drugs	Function	Reference
Nifedipine	Ca^{2+} channel blocker	Weiss et al., 1990
Lidocaine	Na^{+} channel blocker	Bean et al., 1983
E-4031	K^{+} channel blocker	Tamura et al., 2021
Isoproterenol	Beta adrenoceptor agonist	Zhang et al., 2008
Carbachol	Alpha adrenoceptor agonist	Zhao et al., 2019
Doxorubicin	Anthracycline	Sheibani et al., 2022
Sunitinib	High-risk tyrosine kinase inhibitor	Yang and Bu, 2016
Erlotinib	Low-risk tyrosine kinase inhibitor	Liu et al., 2023
Pentamidine	hERG trafficking blocker	Asahi et al., 2019

2018). For this experiment, Test compound dilution series were prepared in a 1 mL deep-well plate as 4× concentrated solutions in the Maintenance Medium and equilibrated in a cell culture incubator for 2 h. All final test concentrations were prepared by a 1:1000 dilution into Maintenance Medium, with a final DMSO concentration of 0.1 %. Refer to Table 6 for the list of CiPA test compounds.

Compound risk categories were assigned according to the reference lists and guidelines published by the Health and Environmental Sciences Institute (HESI) Cardiac Safety Technical Committee, as part of the Comprehensive In Vitro Proarrhythmia Assay (CiPA) initiative. HESI is an international scientific organization that provides consensus-based standards for compound classification based on clinical data and regulatory experience (Gintant et al., 2016; Colatsky et al., 2016). Compounds designated as 'high-risk' are those with well-documented clinical associations with QT prolongation and proarrhythmic outcomes.

Table 6
List of CiPA compounds and their HESI predictions.

Compound	HESI prediction	YBLiCardio
Verampil	Low	79 %
Cisapride	Intermediate	86 %
Diltiazem	Low	93 %
Nitrendipine	Low	97 %
Clozapine	Intermediate	106 %
Loratadine	Low	106 %
Clarithromycin	Intermediate	107 %
Metoprolol	Low	109 %
Risperidone	Intermediate	111 %
Tamoxifen	Low	113 %
Nifedipine	Low	113 %
Terfenadine	Intermediate	116 %
Ondansetron	Intermediate	122 %
Mexiletine	Low	124 %
Pimozide	Intermediate	130 %
Ranolazine	Low	133 %
Chlorpromazine	Intermediate	133 %
Astemizole	Intermediate	139 %
Dofelitide	High	165 %
Ibutilide	High	166 %
Droperidol	Intermediate	173 %
Vandetanib	High	176 %
Azimilide	High	176 %
Domperidone	Intermediate	182 %
Disopyramide	High	217 %
Quinidine	High	249 %
Sotalol	High	275 %
Bepridil	High	344 %

2.14. Cell seeding and maintenance for CiPA assay

Each well of the 96 well CardioExcyte plate was seeded with 100 μL of the cell suspension using a 12-channel electronic pipette (INTEGRA VIAFLO), resulting in a cell density of 85,000 cells per well. Approximately 18–20 h after seeding (Day 1), the plating medium was replaced with 200 μL of pre-warmed Maintenance Medium. From Day 3 onward, a complete medium change was performed every second day. For this purpose, the medium was aspirated from rows A-D using a single-channel aspiration system, and 200 μL of fresh, pre-warmed medium was added to each well using a 12- channel electronic pipette. The same procedure was subsequently repeated with rows E-H.

2.15. Instrumentation and technology

In Electric Field Potential (EFP) mode, the CardioExcyte 96 records extracellular signals from each of the 96 wells, similar to systems that utilize microelectrode arrays (Supplementary Fig. 7). For monitoring high-resolution and low-noise EFP signals, a theoretically uninterrupted cell monolayer must be plated in the wells of the CardioExcyte 96 sensor plate, so that the cleft between the electrode and the monolayer is separated from the remaining medium by a high sealing resistance. During synchronized electrical activity of the monolayer, ions released by the cells are accumulate in the cleft, thereby changing its potential relative to the surrounding medium, which is set to zero potential by the reference electrode. The charge buildup in the cleft is released through the seal resistance, but due to its relatively high value, a voltage can be detected between the sensing electrode beneath the excited cell layer and the reference electrode directly conducting the medium. The large electrode, with its integrating characteristic, sums up the extracellular signals from a greater number of cells and provides the user with an EFP signal representing the average electrical activity of the cells in the respective well.

2.16. Definition of endpoints

The compounds were tested at four different concentrations. Effects were measured as dynamic changes in the beat patterns recorded by means of Electric Field Potential (EPF) sensing. For the assessment of QT prolongation, the time interval between the Sodium spike and the t-wave was assessed.

2.17. Statistical methodology

All statistical analyses were performed using the Wilcoxon–Mann–Whitney test. This nonparametric method was selected for the following reasons:

- Biological replicates ($n = 3$–5 per condition) did not follow a normal distribution, as determined by the Shapiro–Wilk test ($p < 0.05$).
- Sample sizes were limited due to the nature of high-content cardiotoxicity screening.
- The Wilcoxon–Mann–Whitney test does not assume normality and is well-suited for small sample sizes, thus providing a robust approach under these experimental constraints.

3. Results

3.1. Development of a protocol for efficient generation of Cardiomyocytes from hiPSCs

Our optimized protocol generated functional cardiomyocytes from hiPSCs with high reproducibility, achieving >85 % cardiac troponin T (CTNT)-positive cells by day 15 of differentiation (Fig. 1A). Key morphological transitions correlated with developmental stages: early differentiation (days 0–3) featured tightly packed cell colonies, followed

by a progressive shift to a dispersed, fibroblast-like morphology (days 4–7). By day 10, cultures self-organized into synchronously contracting networks (Fig. 1B; Supplementary Video 1), with contraction rates averaging 45 ± 8 beats per minute under baseline conditions.

Spontaneous contractile activity was first observed in a substantial proportion of cells by day 8 of differentiation. The percentage of beating cells increased steadily, reaching a plateau by day 15 and remaining stable thereafter. Cardiomyocytes were harvested and cryopreserved at this stage for subsequent experiments. Upon thawing, the cells were maintained on Matrigel-coated dishes for 3–4 days, during which they regained their typical morphology and spontaneous contractility (Supplementary Video 2), enabling reliable downstream characterization and toxicity screening.

Phase contrast images: Phase contrast images were captured on Days 0, 4, 10, and 15 to monitor iPSCs differentiation into cardiomyocytes. Additionally, Day 20 images depict mature cardiomyocytes obtained by thawing Day 15 cells and cultured them for five more days post-thaw also contribute for CM maturation (Fig. 1B).

3.2. Expression of cardiac markers in hiPSC-derived cardiomyocytes

To confirm the cardiomyocyte identity of differentiated cells, immunocytochemistry was performed on Day 20 YBLiCardio cells to assess the expression of cardiac-specific markers. Cardiac troponin T (CTNT), a subunit of the troponin complex that acts as a calcium-sensitive molecular switch regulating striated muscle contraction (Bhavsar et al., 1996), was localized specifically to the spontaneously contracting regions of the culture (Fig. 1D). In addition to CTNT, the expression of other key contractile proteins, including alpha-actinin, myosin regulatory light chain 2v (MLC2v), and myosin regulatory light chain 2a (MLC2a), was also detected in the hiPSC-derived YBLiCardio population (Fig. 1D). To quantify the purity of YBLiCardio cultures, cells were stained with CTNT as an internal cardiomyocyte marker (Fig. 1C). Flow cytometry analysis revealed that 91.0 ± 8 % of the cells were CTNT-positive, 93.1 ± 2.94 % were alpha-actinin-positive, and 80.5 ± 8 % and 79.9 ± 9 % of the cells expressed MLC2v and MLC2a, respectively (Fig. 1C).

The gene expression profiles of hiPSC-derived YBLiCardio (Day 20) were compared to those of undifferentiated hiPSCs and adult human heart RNA, which served as a positive control. A panel of cardiac-specific genes was analyzed, including myofilament protein genes such as cardiac troponin T (CTNT), α-myosin heavy chain (*MYH7*), myosin light chain 2 ventricular isoform (*MYL2*), and Mesoderm Posterior 1 (MESP1). *qPCR* assays demonstrated that cardiac-specific transcripts were undetectable in undifferentiated hiPSCs and early-stage differentiated cultures but increased significantly after Day 15 of differentiation (Fig. 2A). In contrast, the expression of *hTERT*, a gene highly expressed in undifferentiated pluripotent stem cell cultures (Xu et al., 2001; Lebkowski et al., 2001), decreased progressively during differentiation (data not shown). (See Figs. 3 and 4.)

3.3. Comparative gene expression profiling of iPSC-derived cardiomyocytes and human heart tissue

To evaluate the transcriptomic fidelity of iPSC-derived cardiomyocytes (YBLI-Cardio) to native heart tissue, we performed a comparative analysis of normalized $\log_{10}$ gene expression values across a panel of cardiac-enriched and functionally relevant genes. Samples were collected at two key differentiation timepoints: Day 15 and Day 30. These were compared against reference expression levels in human

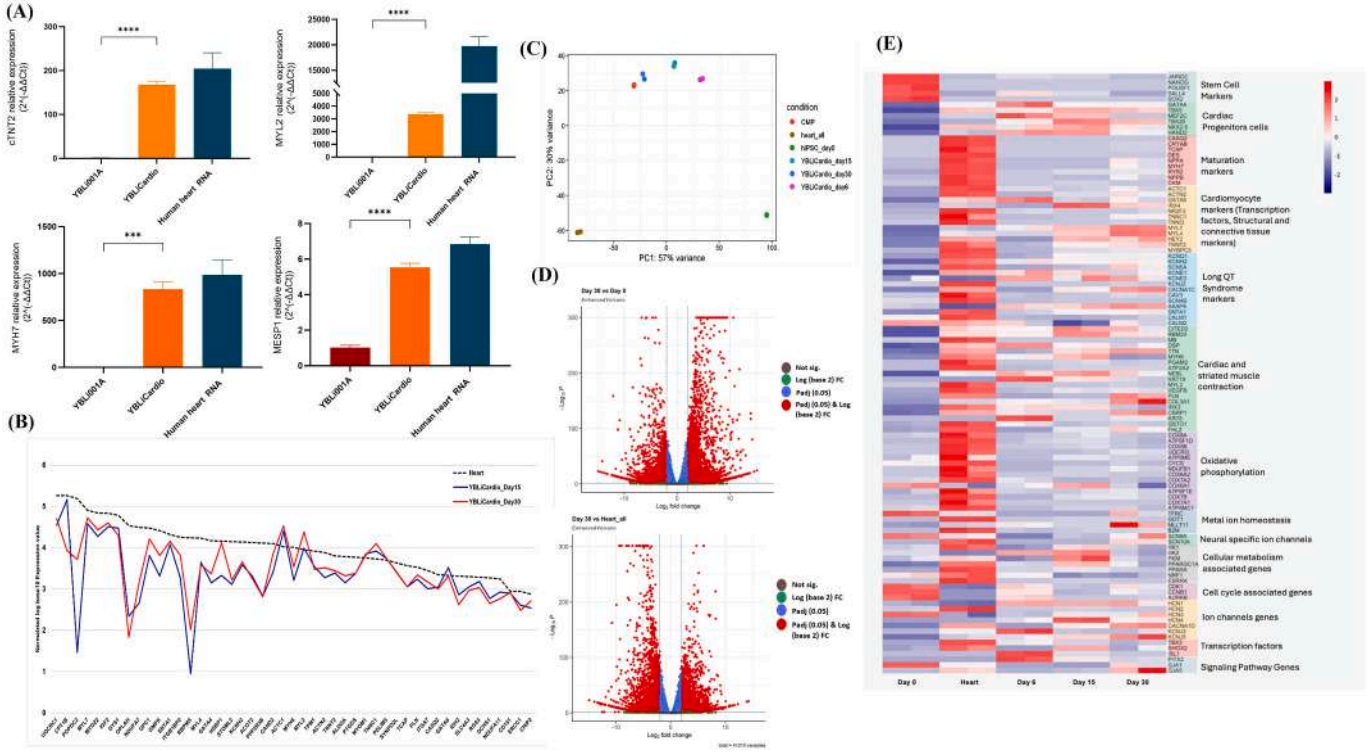

Fig. 2. A) RT-PCR analyses of YBLiCardio for cardiac specific markers CTNT2, MYL2, MYL7, and MESP1. B) Genomic expression profile for YBLiCardio compared with that of adult human cardiac tissue. C) Representation of the principal component analysis (PCA) plot used to denote the sample-to-sample variation. The X and Y-axes represent the first (57 %) and second (30 %) principal components, respectively. D) Volcano plot showing the statistical significance (*p*-value) versus magnitude of change (fold change). X axis represents the magnitude of change in gene expression and Y axis reflects the statistical significance. E) Heatmap of expression levels of specific gene sets. Rows correspond to different genes, and columns represent conditions. Colour intensity indicates expression levels (red = high, blue = low). Shades indicate expressions magnitude. (For interpretation of the references to colour in this figure legend, the reader is referred to the web version of this article.)

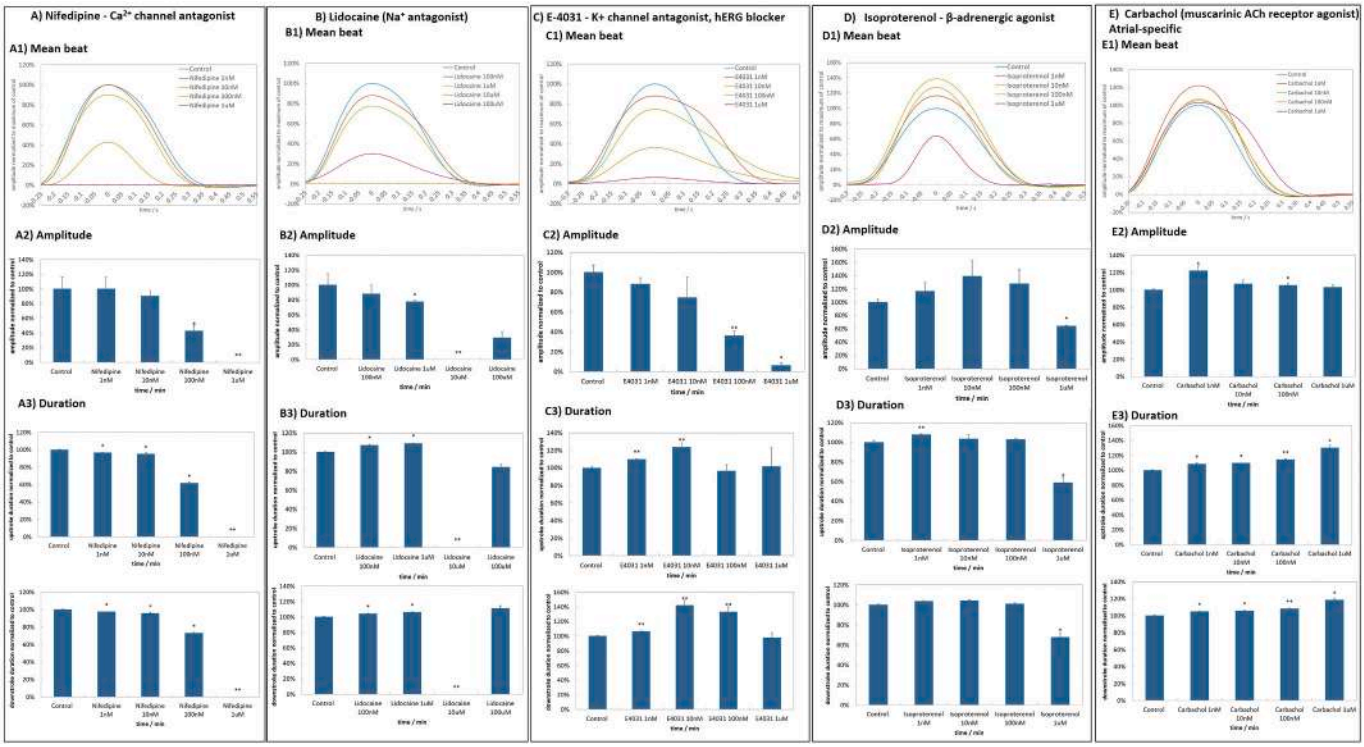

Fig. 3. Acute electrophysiological responses of hiPSC-derived cardiomyocytes to gold-standard reference compounds. Representative data are shown for five pharmacological agents:
(A) Nifedipine (Ca^{2+} channel antagonist), (B) Lidocaine (Na^{+} channel antagonist), (C) E-4031 (K^{+} channel antagonist, hERG blocker), (D) Isoproterenol (β-adrenergic agonist), and (E) Carbachol (muscarinic ACh receptor agonist, atrial-specific). For each compound, the mean beat waveform (A1–E1), amplitude (A2–E2), and duration (A3–E3) were analyzed. Mean beat traces represent normalized average contractility waveforms under control and treated conditions at increasing concentrations (1 nM to 1 μM). Bar plots show quantification of contractility amplitude and duration relative to control (mean ± SD, $n = 3$–5 independent experiments). $^{*}P < 0.05$, $^{*}P < 0.01$ compared to control, by one-way ANOVA with Dunnett's post-hoc test. (For interpretation of the references to colour in this figure legend, the reader is referred to the web version of this article.)

heart tissue.

As illustrated in Fig. 2B, the majority of cardiac-specific genes exhibited similar expression trends between the YBLI-Cardio samples and native heart tissue, with greater alignment was observed at Day 30. Key structural and contractile markers such as TNNT2, MYH6, and ACTN2 were robustly expressed in both Day 15 and Day 30 cardiomyocytes, approaching expression levels observed in the heart. However, certain transcriptional regulators and developmental genes, including TBX5 and NKX2–5, displayed slightly lower expression levels relative to the heart, particularly at Day 15, indicating ongoing maturation.

Notably, Day 30 cardiomyocytes (red line) consistently showed higher expression of several key genes, including MYL2, CASQ2, and CAMK2D, compared to Day 15 (blue line), suggesting progressive maturation toward a more adult-like cardiomyocyte phenotype. Conversely, a few genes such as HAND1 and TBX18 showed diminished expression in iPSC-derived cells relative to the native heart, potentially reflecting developmental stage-specific differences or incomplete recapitulation of all cardiac subtypes (Fig. 2B).

Overall, these data highlight a time-dependent maturation of the iPSC-derived cardiomyocytes, with transcriptional profiles that increasingly resemble native cardiac tissue by Day 30.

3.4. RNA sequencing reveals maturation trajectory in hiPSC-derived cardiomyocytes

A principal component analysis (PCA) plot was generated to visualize the overall variance in gene expression between the samples (Fig. 2C). The PCA plot shows the clustering of samples based on their transcriptional profiles, where each point represents a sample and the distance between points indicates the degree of similarity in gene expression. PC1 accounts for 57 % of the variance, while PC2 accounts for 30 %. The plot reveals distinct clustering patterns: hiPSC_day0 samples are separated from the rest, while CMP, YBLiCardio_day6, YBLiCardio_day15, YBLiCardio_day30, and heart all samples cluster closer together.

To identify significant changes in gene expression between D30 and D0, and D30 and heart RNA, volcano plots were utilized (Fig. 2D). These plots display the log2 fold change in gene expression against the negative log10 of the adjusted *p*-value for each gene. Genes with statistically significant differential expression (adjusted p-value <0.05) and substantial fold changes are highlighted. In the D30 vs D0 volcano plot, a substantial number of genes are upregulated and statistically significant. The volcano plot for D30 vs heart RNA shows a similar trend, with a greater number of upregulated genes exhibiting high significance compared to downregulated genes. This indicates that the gene expression profile of D30 cells is more similar to that of heart tissue. Gene expression changes between other time points are detailed in the supplementary information (Supplementary figure-1).

To determine the gene expression profiling of hiPSC-derived YBLiCardio with human heart RNA and parental hiPSCs, we performed RNA sequencing analysis. Results of RNA sequencing analysis showed decreased expression of pluripotent markers (e.g., NANOG, SOX2) in YBLiCardio. The expression levels of maturation marker genes (e.g., MYH7, CRYAB, NPPA, NPPB) compared with undifferentiated hiPSCs. The cardiac progenitor markers (e.g., GATA4, TBX5, MEF2C, NKX2.5, and HAND2) decreased, while the expression of cardiac transcription factors and structural elements (e.g., CTNT, ACTC1/ACTN2, IRX4, and

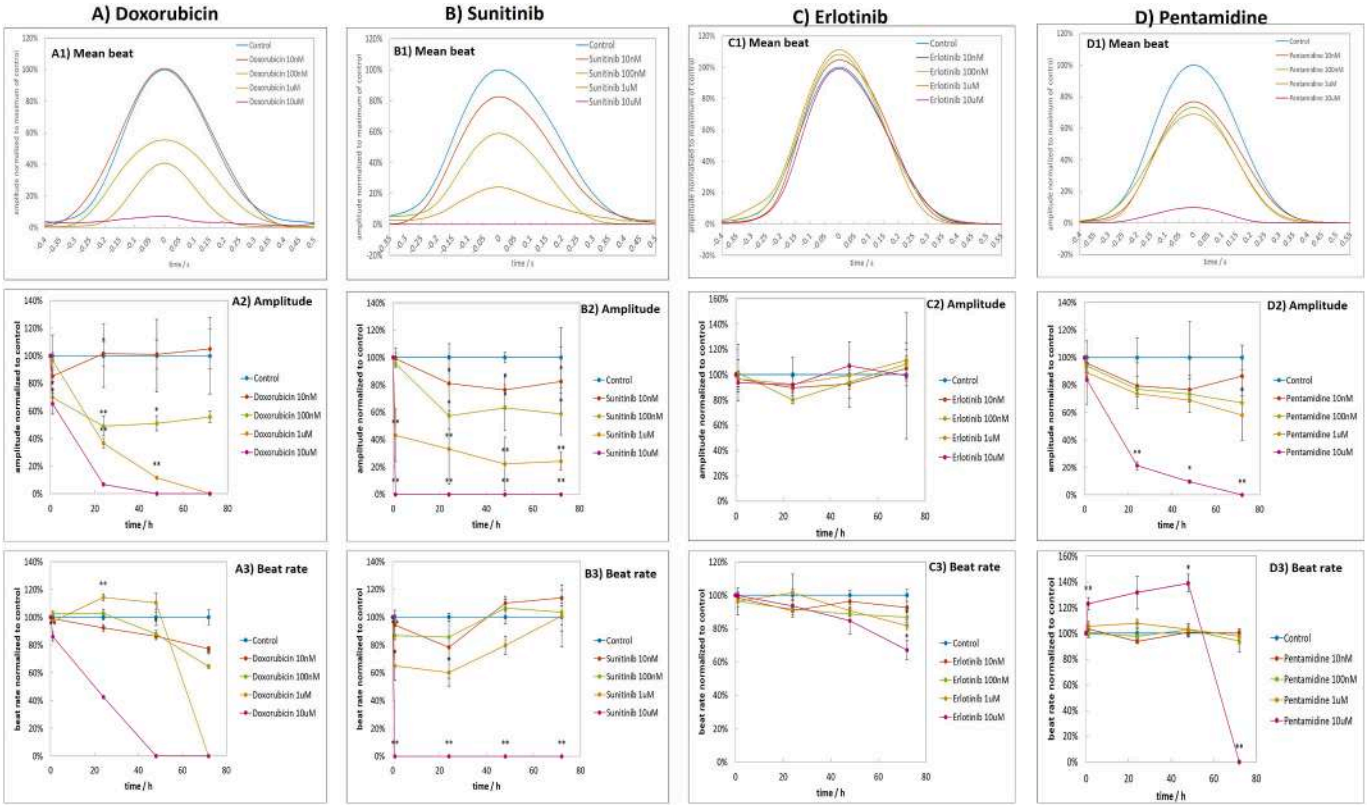

Fig. 4. Chronic cardiotoxic effects of Doxorubicin, Sunitinib, Erlotinib, and Pentamidine on YBLiCardio cells. (A–D) Representative traces of mean beat profiles normalized to peak amplitude are shown for each compound: Doxorubicin (A1), Sunitinib (B1), Erlotinib (C1), and Pentamidine (D1). (A2–D2) Quantification of contraction amplitude over 72 h. (A3–D3) Quantification of beat rate over 72 h. Each compound was tested at 10 nM, 100 nM, 1 μM, and 10 μM concentrations. Doxorubicin and Sunitinib induced concentration-dependent decreases in amplitude and altered beat rate, with complete beat cessation observed at 10 μM. Erlotinib showed no significant effect on amplitude or beat rate across all concentrations. Pentamidine caused a gradual, concentration-dependent decline in amplitude and eventual cessation of beating at the highest concentration.
Data represent mean ± SD from ≥3 biological replicates. Statistical significance relative to control: $*p < 0.05$, $**p < 0.01$ (two-way ANOVA with post hoc multiple comparisons).

MYL4/MYL7) increased with the time of differentiation, displaying a similar pattern to the human heart RNA (Fig. 2E). Genes related to cardiac energy metabolism and oxidative phosphorylation also contribute to CM maturation. The genes (e.g., NPPA, MYL2, COLA31, CSRP1) associated with heart development, muscle cell development, and cardiac muscle contraction, showed a similar pattern of expression with the human heart. hiPSC-derived CM expressed recognized long QT syndrome (LQTS) genes, including KCNQ1, KCNH2, and SCN5A, in addition to other ion channels at 15 and 30 days. (Fig. 2E). The expression of pacemaker-related genes, including *HCN1, HCN2,* and *HCN4*, was low in undifferentiated hiPSCs (Day 0) but progressively increased during differentiation. Notably, their expression was markedly upregulated in the adult human heart sample, serving as a positive control. A significant upregulation of these genes was also observed at Days 15 and 30 of differentiation, indicating maturation toward a pacemaker-like cardiomyocyte phenotype (Fig. 2E).

3.5. Acute compound reactions

Nifedipine, a dihydropyridine derivative and L-type Ca^{2+} channel blocker (Weiss et al., 1990) was used to evaluate calcium handling in cells across a concentration range of 1 nM to 1 μM (Fig. 3A1). As anticipated, nifedipine elicited concentration-dependent effects on calcium transients. At 1 nM and 10 nM, minimal changes were observed. However, at 100 nM amplitude was reduced to approximately 40 % of control, and at 1 μM, spontaneous beating activity was completely abolished (Fig. 3A2). Nifedipine also induced a concentration-dependent shortening of beat duration, with the most pronounced effect at 100 nM, where upstroke and downstroke durations were reduced to 60 % and 70 % of control, respectively (Fig. 3A3). Similar concentration-dependent reductions were observed in the area under the curve (AUC) and the slopes of the upstroke and downstroke phases (Supplementary Fig. 2A1 & 2A2), consistent with the overall suppression of calcium transient kinetics.

Lidocaine, a sodium channel blocker (Bean et al., 1983), was evaluated at concentrations from 100 nM to 100 μM. The compound produced concentration-dependent negative inotropic effects, with notable reductions in amplitude at concentrations ≥1 μM, culminating in cessation of spontaneous beating at 10 μM and above (Fig. 3B1). At 100 μM, some wells exhibited weak, irregular concentrations with markedly reduced amplitude (Fig. 3B2). Beat rate remained largely unaffected at concentrations up to 1 μM, while higher concentrations induced arrhythmic activity. Lidocaine also caused a mild but statistically significant prolongation of both upstroke and downstroke durations, prior to complete cessation of beating at 10 μM (Fig. 3B3). Consistent with these findings, the area under the curve (AUC) decreased in parallel with amplitude reductions, and the slopes of the upstroke and downstroke phases followed similar concentration-dependent trends (Supplementary Fig. 2B1 & 2B2).

E-4031, a selective hERG channel blocker (Tamura et al., 2021), was tested at concentrations ranging from 1 nM to 1 μM. The compound produced negative inotropic effects and marked prolongation of beat duration, with arrhythmic events emerging at concentrations of 100 nM and above (Fig. 3C1). Amplitude was reduced to approximately 40 % of

control at 100 nM, and was nearly abolished at 1 μM. A concentration-dependent decrease in beat rate was observed, although at 1 μM, persistent fibrillatory activity resulted in an apparent increase in event frequency, reaching ~150 % of control (Fig. 3C2). E-4031 also induced significant prolongation of both upstroke and downstroke durations; however, arrhythmic activity at higher concentrations contributed to overall shortening of duration metrics (Fig. 3C3). AUC and slope analyses mirrored these trends, with substantial reductions noted at higher concentrations (Supplementary Fig. 2C1 & 2C2).

Isoproterenol, β-adrenergic agonist (Zhang et al., 2008) was applied at concentrations ranging from 1 nM to 1 μM. It evaluates positive inotropic responses. Significant positive inotropic effects were observed at concentrations up to 100 nM, as evidenced by increased amplitude (Fig. 3D1). However, at 1 μM, amplitude decreased, likely due to overstimulation-induced desensitization (Fig. 3D2). Beat rate remained stable at lower concentrations but increased markedly, reaching approximately 200 % of control at 1 μM. Upstroke and downstroke durations were only slightly affected at concentrations up to 100 nM but were significantly shortened at 1 μM (Fig. 3D3). The area under the curve (AUC) tracked closely with amplitude changes, showing a pronounced decline at 1 μM. Similarly, the slopes of the upstroke and downstroke phases mirrored the amplitude trends (Supplementary Fig. 2D1 & 2D2). Carbachol, an α-adrenergic agonist (Zhao et al., 2019), was applied to assess chamber-specific functional responses in YBLiCardio cells. The compound induced a concentration dependent increase in concentration duration, with a ~ 25 % prolongation observed, suggesting a mixed atrial and ventricular phenotype (Fig. 3E1). Amplitude was largely unaffected across concentrations, except at 1 nM, where a significant increase was detected (Fig. 3E2). Carbachol also produced a concentration-dependent decrease in beat rate, consistent with prolonged beat durations. At 1 μM, contraction duration increased to approximately 130 % of control (Fig. 3E3). Correspondingly, the area under the curve (AUC) steadily increased, reflecting the extended durations, while upstroke and downstroke slopes followed trends consistent with amplitude and duration changes, with peak values observed at 1 nM (Supplementary Fig. 2E1 & 2E2).

3.6. Chronic compound reactions

Doxorubicin, an anthracycline derivative, was used to evaluate chronic cardiotoxicity through assessment of cardiac energetics when treated for 72 h. As expected, it elicited time- and concentration-dependent negative inotropic effects (Sheibani et al., 2022). A concentration-dependent reduction in contraction amplitude was observed, with no significant change at 10 nM, a decrease to ~60 % of control at 100 nM after 24 h (Fig. 4A1),), and progressive reduction at 1 μM leading to beat cessation by 72 h. At 10 μM, amplitude declined to ~10 % of control by 24 h, with beat cessation occurring at 48 h (Fig. 4A2). Beat rate remained largely unchanged at ≤100 nM but showed a transient increase at 1 μM before cessation at 72 h; at 10 μM, it gradually decreased and ceased by 48 h (Fig. 4A3). Upstroke and downstroke durations were minimally affected at ≤100 nM; however, higher concentrations induced shortening of both phases, independent of concentration (Supplementary Fig. 3A1). The area under the curve (AUC) closely paralleled amplitude reductions (Supplementary Fig. 3A2), while the slopes of upstroke and downstroke phases declined in a time- and concentration-dependent manner (Supplementary Fig. 3A3).

Sunitinib, a tyrosine kinase inhibitor with a well- documented cardiotoxic profile (Yang and Bu, 2016), induced a concentration-dependent reduction in contraction amplitude, with immediate effects observed at higher concentrations (Fig. 4B1,4B2). At 10 μM, cells ceased beating within the first hour. At lower concentrations, amplitude declined significantly within the first 24 h and remained suppressed but stable through 72 h (Fig. 4B3). Sunitinib also reduced beat rate during the first 24 h, followed by a gradual recovery to baseline levels by 72 h. At 10 μM, beat rate dropped precipitously, coinciding with early cessation of beating (Fig. 4B3). The upstroke phase was initially prolonged; however, with sustained exposure, upstroke duration shortened. The downstroke phase showed early shortening followed by a return to near-control values (Supplementary Fig. 3B1). AUC declined in parallel with amplitude, demonstrating a time- and concentration-dependent effect (Supplementary Fig. 3B2). Slopes of both contraction and relaxation phases were reduced in a pattern consistent with amplitude suppression, with complete beat cessation observed at the highest concentration (Supplementary Fig. 3B3). Erlotinib, a tyrosine kinase inhibitor with a low cardiotoxicity profile (Liu et al., 2023), had no significant effect on the contractile properties of YBLiCardio cells at any of the tested concentrations (Fig. 4C1). Neither concentration amplitude nor beat rate was altered, even at the highest concentration after 72 h of exposure (Fig. 4C2 & 4C3). Similarly, erlotinib did not affect the durations of the upstroke and downstroke phases (Supplementary Fig. 4A1), nor did it impact the area under the curve (AUC) or the slopes of contraction and relaxation phases over the 72-h period (Supplementary Fig. 4A2, 4A3) 4, indicating a lack of significant cardiac functional effects.

Pentamidine, used to evaluate chronic cardiotoxicity associated with hERG trafficking disruption (Asahi et al., 2019), exhibited time- and concentration-dependent negative effects on contractile function. A concentration-dependent decrease in contraction amplitude was observed, with 10 μM causing a gradual decline leading to beat cessation at 72 h (Fig. 4D1, 4D2). Beat rate remained unaffected at concentrations up to 1 μM; however, at 10 μM, an initial increase in beat rate was followed by complete cessation at 72 h (Fig. 4D3). Upstroke and downstroke durations were unchanged at ≤1 μM, but both were shortened at 10 μM prior to beat cessation (Supplementary Fig. 4B1). AUC reductions mirrored amplitude decline (Supplementary Fig. 4B2), and slopes of both contraction and relaxation phases decreased in a concentration-dependent manner, reflecting reduced amplitude while durations remained relatively preserved at lower concentrations (Supplementary Fig. 4B3).

3.7. HESI CiPA compound effects on YBLiCardio cells

To evaluate the proarrhythmic risk of test compounds, we measured changes in field potential duration (FPD) in human iPSC-derived cardiomyocytes (YBLiCardio cells) and normalized the values to control (DMSO-treated) conditions. Based on the extent of FPD prolongation, compounds were stratified into three risk categories: low (79 %–113 %), intermediate (113 %–139 %), and high (165 %–344 %) (Fig. 5A) (Blinova et al., 2017; Blinova et al., 2018). YBLiCardio cells exhibited pharmacological responses consistent with those observed in the HESI CiPA study. High-risk compounds, as pre-classified by HESI CiPA, induced the most pronounced QT interval prolongation, ranging from 165 % to 344 % (Fig. 5D). Notably, droperidol (173 %) and domperidone (182 %), although categorized as intermediate-risk, were identified as high-risk compounds in this assay, aligning with previous findings (Nguyen et al., 2017) (Fig. 5C). Low-risk compounds, including mexiletine and ranolazine, demonstrated minimal FPD prolongation, consistent with expectations (Fig. 5B). Interestingly, chlorpromazine exhibited higher predictive accuracy in YBLiCardio cells compared to other cell models (Fig. 5E, Supplementary Fig. 5). Moreover, the full panel of compounds tested yielded risk classifications concordant with those reported in the original CiPA ring trial (Fig. 5E, Supplementary Figs. 5 & 7), supporting the predictive validity of this iPSC-derived cardiomyocyte assay system.

4. Discussion

This study introduces YBLiCardio—a highly enriched, functionally mature hiPSC-derived cardiomyocyte platform—tailored for predictive cardiotoxicity testing under the CiPA framework. While several

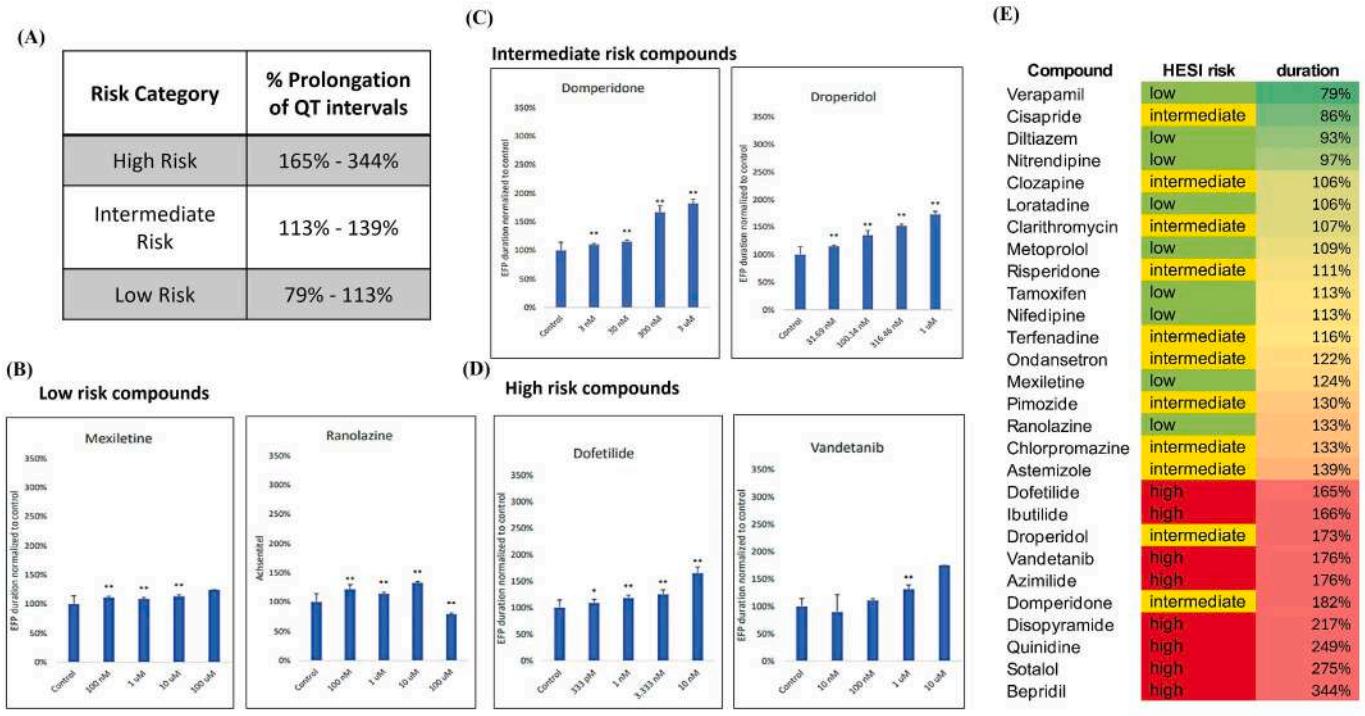

Fig. 5. Classification of compound-induced QT prolongation risk in YBLiCardio cells. (A) Table summarizing QT interval prolongation thresholds used to classify compounds as high, intermediate, or low risk, based on the percentage of field potential duration (FPD) prolongation relative to control. (B—D) Bar graphs showing dose-dependent FPD changes induced by representative (B) low-risk (Mexiletine, Ranolazine), (C) intermediate-risk (Domperidone, Droperidol), and (D) high-risk (Dofetilide, Vandetanib) compounds. FPD values were normalized to DMSO-treated controls. (E) Heatmap of all tested compounds ranked by normalized FPD duration. Compounds are annotated with their HESI CiPA risk classification and grouped based on increasing QT prolongation. Green, yellow, and red backgrounds indicate low, intermediate, and high risk, respectively.
Data are represented as mean ± SD (n = 3–5 independent experiments). *$p < 0.05$, **$p < 0.01$ compared to control.

protocols exist for cardiomyocyte differentiation, our optimization using STEMdiff™ medium combined with temporal Wnt signaling modulation has resulted in robust, reproducible generation of cardiomyocytes with high purity and functional maturity. The reproducibility and yield of >90 % CTNT+ cells indicate the potential for translational application in preclinical drug screening pipelines.

Importantly, our transcriptional profiling places YBLiCardio on a maturation trajectory that closely parallels adult human heart tissue, as evidenced by RNA-seq clustering and the expression convergence of over 2800 genes with adult cardiac tissue. This maturation fidelity addresses a critical limitation in existing hiPSC-CM models, which often remain developmentally immature and therefore poorly predictive of adult cardiac responses. In contrast to previous reports, we observed strong expression of ventriular-specific markers (e.g., MYL2, MLC2v) and functionally relevant ion channel genes (e.g., SCN5A, KCNQ1, KCNH2), which are often underrepresented in other commercial platforms. This establishes YBLiCardio not only as a structurally relevant but also electrophysiologically competent model.

The functional validation with acute and chronic drug exposures confirmed the system's physiological relevance. In particular, the CiPA compound panel demonstrated that YBLiCardio recapitulates expected proarrhythmic responses, such as QT prolongation by E-4031, and shows enhanced sensitivity in detecting high-risk compounds like droperidol and domperidone-findings consistent with and extending those of Nguyen et al. (2017). Notably, YBLiCardio was able to accurately detect chlorpromazine-associated risk, where other hiPSC-CM models have shown limitations. While these results highlight the potential of YBLiCardio to improve the detection of certain pharmacological risks, especially in the case of chlorpromazine, further studies are warranted to determine whether this enhanced predictive capacity extends broadly across diverse and complex pharmacological scenarios.Furthermore, the distinct chronic toxicity responses to agents like doxorubicin and sunitinib underscore YBLiCardio's utility in modeling progressive cardiomyopathy phenotypes—an area often overlooked in short-term assays. The ability to track contractile function and recovery post-drug exposure over 72 h represents a critical innovation in modeling delayed cardiotoxic effects.

The current YBLiCardio platform is a robust and reliable tool for assessing the preclinical cardiotoxicity of chemical entities. It not only enables accurate prediction of compound toxicity in conventional 2D static cultures, but also demonstrates the capability to support the development of 3D cardiac structures. This advancement highlights the potential of YBLiCardio as a more physiologically relevant in vitro system, offering a promising alternative to animal models in preclinical cardiotoxicity assessments. These findings warrant further investigation and validation.The initial findings with YBLiCardio cardiomyocytes shows seamless integration into FluidForm's FRESH cardiac tissue printing workflow (Supplementary Video 3 and 4). Where preparation of YBLiCardio into a high-density bioink was straightforward, with no issues observed during the process—such as cell clumping, excessive debris, or needle clogging. The bioink exhibited excellent extrusion characteristics, enabling the production of high-fidelity cardiac tissue constructs. In culture, printed YBLiCardio tissues exhibited expected morphological and functional behaviors, including notable compaction from the initial printed geometry to a stable configuration around anchoring pillar. By day 7 of culture, all printed constructs displayed visually apparent, synchronous contractions across the tissue. These observations suggest robust cellular viability and, more specifically, a high proportion of functional cardiomyocytes capable of forming an aligned and contractile syncytium (Supplementary video 3 for Day 7 and 14 cardiac patch). These systems incorporate multiple cell types and are engineered to provide structural, electrical, and biochemical

environments that more closely mimic the native myocardium. By integrating 3D scaffolds, mechanical stretch, and electrical pacing, these advanced platforms are expected to enhance maturation and better reflect the in vivo human cardiac physiology.

The importance of advancing such physiologically relevant in vitro systems is underscored by the The FDA Modernization Act 2.0 and 3.0 aim to modernize drug development by reducing reliance on animal testing and encouraging alternative methods., including hiPSC-based models—for drug developmet and safety testing. This legislative shift amplifies the significance of models like YBLiCardio, which can serve as a human-relevant, ethically responsible, and highly scalable platform for early-stage drug screening and regulatory decision-making.

In the context of existing literature, YBLiCardio advances the field by offering:

1. With its high purity, functional maturity, and transcriptional convergence toward adult cardiac tissue, YBLiCardio addresses key limitations of existing hiPSC-derived cardiomyocyte platforms—particularly developmental immaturity and lack of predictive fidelity.
2. Its validated performance under the CiPA paradigm, coupled with superior sensitivity in detecting proarrhythmic and cardiotoxic responses—including compounds missed by other models—underscores its translational value.
3. YBLiCardio seamless integration into 3D bioprinting workflows and ability to model chronic drug responses positions it as a next-generation tool suitable for regulatory safety pharmacology.

Collectively, these features position YBLiCardio as a high predictive, robust next-generation cardiotoxicity assessment, with the scope of further expansion in to 3D organoid models with other cell types. YBLiCardio has the potential to develop as a preclinical translational tool to assess the cardiotoxicity and torsedogenic potential of compounds.

5. Conclusion

In summary, YBLiCardio represents a robust, functionally mature hiPSC-derived cardiomyocyte platform that demonstrates strong predictive fidelity for proarrhythmic and cardiotoxic risk assessment. Our findings show that YBLiCardio not only aligns with the outcomes of the HESI CiPA study but also offers enhanced sensitivity—reclassifying compounds such as droperidol and domperidone as higher-risk and accurately identifying the cardiotoxic potential of chlorpromazine, which was previously undetected by other hiPSC-CM models. The platform's high purity ventricular marker expression, and electrophysiological competence further validate its suitability for preclinical drug screening. Together, these attributes establish YBLiCardio as a scalable, ethically responsible, and translationally relevant tool that aligns with the goals of the FDA Modernization Acts 2.0 and 3.0. As such, YBLiCardio holds strong potential for widespread adoption in early-stage drug development, regulatory safety pharmacology, and future integration into complex 3D cardiac organoid platforms.

Supplementary data to this article can be found online at https://doi.org/10.1016/j.tiv.2025.106100.

CRediT authorship contribution statement

Vijay Bhaskar Reddy Konala: Writing – original draft, Methodology, Investigation, Formal analysis, Data curation, Conceptualization. **Rutuja Kuhikar:** Software, Methodology, Investigation, Formal analysis, Data curation. **Shruti More:** Methodology, Data curation. **Matthias Gossmann:** Software, Methodology, Data curation. **Bettina Lickiss:** Software, Data curation. **Peter Linder:** Software, Data curation. **Jaganmay Sarkar:** Methodology. **Paresh Bhanushali:** Supervision. **Amit Khanna:** Writing – review & editing, Supervision, Project administration.

Funding

This work was funded by Yashraj Biotechnology Limited, Navi Mumbai, Maharastra, India.

Declaration of competing interest

The authors declare that they have no known competing financial interests or personal relationships that could have appeared to influence the work reported in this paper.

Acknowledgments

The authors gratefully acknowledge the valuable contributions and constructive critiques from the entire Yashraj Biotechnology team and the Scientific Advisory Committee of YBL throughout this project. Special thanks are extended to Mibiome for providing sequencing and data analysis services. We also acknowledge the Indian Institute of Technology (IIT) Bombay for their support with confocal imaging. Additionally, we would like to thank FluidForm for utilizing our YBLiCardio platform to test their FRESH printing technology in the development of cardiac patches.

Data availability

Data will be made available on request.

References

Andrews, S., 2010. FastQC: a quality control tool for high throughput sequence data. Available online at http://www.bioinformatics.babraham.ac.uk/projects/fastqc.

Asahi, Y., Nomura, F., Abe, Y., Doi, M., Sakakura, T., Takasuna, K., Yasuda, K., 2019. Electrophysiological evaluation of pentamidine and 17-AAG in human stem cell-derived cardiomyocytes for safety assessment. Eur. J. Pharmacol. 5 (842), 221–230. https://doi.org/10.1016/j.ejphar.2018.10.046.

Bean, B.P., Cohen, C.J., Tsien, R.W., 1983. Lidocaine block of cardiac sodium channels. J. Gen. Physiol. 81 (5), 613–642. https://doi.org/10.1085/jgp.81.5.613.

Bhavsar, P.K., Brand, N.J., Yacoub, M.H., Barton, P.J., 1996. Isolation and characterization of the human cardiac troponin I gene (TNNI3). Genomics 35 (1), 11–23. https://doi.org/10.1006/geno.1996.0317.

Blinova, K., Stohlman, J., Vicente, J., Chan, D., Johannesen, L., Hortigon-Vinagre, M.P., Zamora, V., Smith, G., Crumb, W.J., Pang, L., Lyn-Cook, B., Ross, J., Brock, M., Chvatal, S., Millard, D., Galeotti, L., Stockbridge, N., Strauss, D.G., 2017. Comprehensive translational assessment of human-induced pluripotent stem cell derived cardiomyocytes for evaluating drug-induced arrhythmias. Toxicol. Sci. 155 (1), 234–247. https://doi.org/10.1093/toxsci/kfw200.

Blinova, K., Dang, Q., Millard, D., Smith, G., Pierson, J., Guo, L., Brock, M., Lu, H.R., Kraushaar, U., Zeng, H., Shi, H., Zhang, X., Sawada, K., Osada, T., Kanda, Y., Sekino, Y., Pang, L., Feaster, T.K., Kettenhofen, R., Stockbridge, N., Strauss, D.G., Gintant, G., 2018. International multisite study of human-induced pluripotent stem cell-derived cardiomyocytes for drug proarrhythmic potential assessment. Cell Rep. 24 (13), 3582–3592. https://doi.org/10.1016/j.celrep.2018.08.079.

Chen, S., 2023. Ultrafast one-pass FASTQ data preprocessing, quality control, and deduplication using fastp. Imeta 2 (2), e107. https://doi.org/10.1002/imt2.107.

Chitrangi, S., Vaity, P., Jamdar, A., Patel, H., Bhatt, S., 2023. Generation of human induced pluripotent stem cell line from PBMCs of healthy donors using integration-free Sendai virus technology. Stem Cell Res. 69, 103062. https://doi.org/10.1016/j.scr.2023.103062.

Colatsky, T., Fermini, B., Gintant, G., Pierson, J.B., Sager, P., Sekino, Y., Strauss, D.G., Stockbridge, N., 2016. The Comprehensive in Vitro Proarrhythmia Assay (CiPA) initiative - update on progress. J. Pharmacol. Toxicol. Methods 81, 15–20. https://doi.org/10.1016/j.vascn.2016.06.002.

Di Marco, A., Gaetani, M., Orezzi, P., Scarpinato, B.M., Silvestrini, R., Soldati, M. Dasdia, T, Valentini L., 1964. "Daunomycin", a new antibiotic of the rhodomycin group. Nature 201 (4920), 706–707. https://doi.org/10.1038/201706a0.

FDA, 2005a. International Conference on Harmonisation; guidance on E14 Clinical Evaluation of QT/QTc Interval Prolongation and Proarrhythmic Potential for Non-Antiarrhythmic Drugs; availability. Notice. Fed. Regist 70, 61134–61135.

FDA, 2005b. International Conference on Harmonisation; guidance on S7B Nonclinical Evaluation of the Potential for Delayed Ventricular Repolarization (QT Interval Prolongation) by Human Pharmaceuticals; availability. Notice. Fed. Regist 70, 61133–61134.

Fermini, B., Hancox, J.C., Abi-Gerges, N., Bridgland-Taylor, M., Chaudhary, K.W., Colatsky, T., Correll, K., Crumb, W., Damiano, B., Erdemli, G., et al., 2016. A new perspective in the field of cardiac safety testing through the comprehensive in vitro

proarrhythmia assay paradigm. J. Biomol. Screen. 21 (1), 1–11. https://doi.org/10.1177/1087057115594589.
Frothingham, R., 2001. Rates of torsades de pointes associated with ciprofloxacin, ofloxacin, levofloxacin, gatifloxacin, and moxifloxacin. Pharmacother. J. Hum. Pharmacol. Drug Ther. 21 (12), 1468–1472. https://doi.org/10.1592/phco.21.20.1468.34482.
Fung, M., Thornton, A., Mybeck, K., et al., 2001. Evaluation of the characteristics of safety withdrawal of prescription drugs from worldwide pharmaceutical Markets-1960 to 1999. Ther. Innov. Regul. Sci. 35, 293–317. https://doi.org/10.1177/009286150103500134.
Funk, K.A., Bostwick, J.R., 2013. A comparison of the risk of QT prolongation among SSRIs. Ann. Pharmacother. 47 (10), 1330–1341. https://doi.org/10.1177/1060028013501994.
Gintant, G., Sager, P.T., Stockbridge, N., 2016. Evolution of strategies to improve preclinical cardiac safety testing. Nat. Rev. Drug Discov. 15 (7), 457–471. https://doi.org/10.1038/nrd.2015.34.
Johannesen, L., Vicente, J., Mason, J.W., Sanabria, C., Waite-Labott, K., Hong, M., Guo, P., Lin, J., Sorensen, J.S., Galeotti, L., et al., 2014. Differentiating drug-induced multichannel block on the electrocardiogram: randomized study of dofetilide, quinidine, ranolazine, and verapamil. Clin. Pharmacol. Ther. 96 (5), 549–558. https://doi.org/10.1038/clpt.2014.155.
Kim, D., Paggi, J.M., Park, C., Bennett, C., Salzberg, S.L., 2019. Graph-based genome alignment and genotyping with HISAT2 and HISAT-genotype. Nat. Biotechnol. 37 (8), 907–915. https://doi.org/10.1038/s41587-019-0201-4.
Køber, L., Torp-Pedersen, C., JJ, McMurray, Gøtzsche, O., Lévy, S., Crijns, H., Amlie, J., Carlsen, J., Dronedarone Study Group, 2008. Increased mortality after dronedarone therapy for severe heart failure. N. Engl. J. Med. 358 (25), 2678–2687. https://doi.org/10.1056/NEJMoa0800456.
Konala, V.B.R., Nandakumar, S., Battu, R., Pal, R., 2020. Derivation of three induced pluripotent stem cell lines under feeder-free culture conditions from peripheral blood mononuclear cells (PBMC) of Indian patients suffering from inherited retinal diseases carrying different mutations. Stem Cell Res. 45, 101757. https://doi.org/10.1016/j.scr.2020.101757.
Kopylova, E., Noé, L., Touzet, H., 2012. SortMeRNA: fast and accurate filtering of ribosomal RNAs in metatranscriptomic data. Bioinformatics 28 (24), 3211–3217. https://doi.org/10.1093/bioinformatics/bts611.
Lebkowski, J.S., Gold, J., Xu, C., Funk, W., Chiu, C.P., Carpenter, M.K., 2001. Human embryonic stem cells: culture, differentiation, and genetic modification for regenerative medicine applications. Cancer J. 7 (2), S83–S93 (PMID: 11777269).
Lee, H.M., Hahn, S.J., Choi, B.H., 2022. The antidiabetic drug rosiglitazone blocks Kv1.5 potassium channels in an open state. Korean J. Physiology Pharmacol. 26 (2), 135–144. https://doi.org/10.4196/kjpp.2022.26.2.135.
Liao, Y., Smyth, G.K., Shi, W., 2014. featureCounts: an efficient general purpose program for assigning sequence reads to genomic features. Bioinformatics 30 (7), 923–930. https://doi.org/10.1093/bioinformatics/btt656.
Liu, Q., Li, S., Qiu, Y., Zhang, J., Rios, F.J., Zou, Z., Touyz, R.M., 2023. Cardiovascular toxicity of tyrosine kinase inhibitors during cancer treatment: potential involvement of TRPM7. Front Cardiovasc Med. 3 (10), 1002438. https://doi.org/10.3389/fcvm.2023.1002438.
Love, M.I., Huber, W., Anders, S., 2014. Moderated estimation of fold change and dispersion for RNA-seq data with DESeq2. Genome Biol. 15 (12), 550. https://doi.org/10.1186/s13059-014-0550-8.
Lundy, S.D., Zhu, W.Z., Regnier, M., Laflamme, M.A., 2013. Structural and functional maturation of cardiomyocytes derived from human pluripotent stem cells. Stem Cells Dev. 22 (14), 1991–2002. https://doi.org/10.1089/scd.2012.0490.
Mamoshina, P., Rodriguez, B., Bueno-Orovio, A., 2021. Toward a broader view of mechanisms of drug cardiotoxicity. Cell Rep Med. 2 (3), 100216. https://doi.org/10.1016/j.xcrm.2021.100216.
Nguyen, N., Nguyen, W., Nguyenton, B., Ratchada, P., Page, G., Miller, P.E., Ghetti, A., Abi-Gerges, N., 2017. Adult human primary cardiomyocyte-based model for the simultaneous prediction of drug-induced inotropic and pro-arrhythmia risk. Front. Physiol. 19 (8), 1073. https://doi.org/10.3389/fphys.2017.01073.
Onakpoya, I.J., Heneghan, C.J., Aronson, J.K., 2016. Post-marketing withdrawal of 462 medicinal products because of adverse drug reactions: a systematic review of the world literature. BMC Med. 4 (14), 10. https://doi.org/10.1186/s12916-016-0553-2.
Ronaldson-Bouchard K, Ma SP, Yeager K, Chen T, Song L, Sirabella D, Morikawa K, Teles D, Yazawa M, Vunjak-Novakovic G. Advanced maturation of human cardiac tissue grown from pluripotent stem cells. Nature. 2018;556(7700):239-243. Doi: https://doi.org/10.1038/s41586-018-0016-3. Epub 2018 Apr 4. Erratum in: Nature. 2019;572(7769):E16-E17. doi:https://doi.org/10.1038/s41586-019-1415-9.
Sager, P.T., Gintant, G., Turner, J.R., Pettit, S., Stockbridge, N., 2014. Rechanneling the cardiac proarrhythmia safety paradigm: a meeting report from the cardiac safety research consortium. Am. Heart J. 167 (3), 292–300. https://doi.org/10.1016/j.ahj.2013.11.004.
Seyhan, A.A., 2019. Lost in translation: the valley of death across preclinical and clinical divide – identification of problems and overcoming obstacles. transl med commun 4, 18. https://doi.org/10.1186/s41231-019-0050-7.
Sheibani, M., Azizi, Y., Shayan, M., Nezamoleslami, S., Eslami, F., Farjoo, M.H., Dehpour, A.R., 2022. Doxorubicin-induced cardiotoxicity: an overview on pre-clinical therapeutic approaches. Cardiovasc. Toxicol. 22 (4), 292–310. https://doi.org/10.1007/s12012-022-09721-1.
Singh, B.N., Connolly, S.J., Crijns, H.J., Roy, D., Kowey, P.R., Capucci, A., Radzik, D., Aliot, E.M., Hohnloser, S.H., EURIDIS and ADONIS Investigators., 2007. Dronedarone for maintenance of sinus rhythm in atrial fibrillation or flutter. N. Engl. J. Med. 357 (10), 987–999. https://doi.org/10.1056/NEJMoa054686.
Stockbridge, N., Morganroth, J., Shah, R.R., Garnett, C., 2013. Dealing with global safety issues : was the response to QT-liability of non-cardiac drugs well coordinated? Drug Saf. 36 (3), 167–182. https://doi.org/10.1007/s40264-013-0016-z.
Tamura, F., Sugimoto, S., Sugimoto, M., Sakamoto, K., Yamaguchi, M., Suzuki, T., Fukuda, K., Ieda, M., Kurokawa, J., 2021. The effect of a synthetic estrogen, ethinylestradiol, on the hERG block by E-4031. Biomolecules 11 (9), 1385. https://doi.org/10.3390/biom11091385.
Tan, C., Tasaka, H., Yu, K.P., Murphy, M.L., Karnofsky, D.A., 1967. Daunomycin, an antitumor antibiotic, in the treatment of neoplastic disease. Clinical evaluation with special reference to childhood leukemia. Cancer 20 (3), 333–353. https://doi.org/10.1002/1097-0142(1967)20:33.0.CO;2-K.
Weiss, J.H., Hartley, D.M., Koh, J., Choi, D.W., 1990. The calcium channel blocker nifedipine attenuates slow excitatory amino acid neurotoxicity. Science 247 (4949 Pt 1), 1474–1477. https://doi.org/10.1126/science.247.4949.1474.
Xu, C., Inokuma, M.S., Denham, J., Golds, K., Kundu, P., Gold, J.D., Carpenter, M.K., 2001. Feeder-free growth of undifferentiated human embryonic stem cells. Nat. Biotechnol. 19 (10), 971–974. https://doi.org/10.1038/nbt1001-971.
Yang, Y., Bu, P., 2016. Progress on the cardiotoxicity of sunitinib: prognostic significance, mechanism and protective therapies. Chem. Biol. Interact. 25 (257), 125–131. https://doi.org/10.1016/j.cbi.2016.08.006.
Zhang, J., Knapton, A., Lipshultz, S.E., Weaver, J.L., Herman, E.H., 2008. Isoproterenol-induced cardiotoxicity in Sprague-dawley rats: correlation of reversible and irreversible myocardial injury with release of cardiac troponin T and roles of iNOS in myocardial injury. Toxicol. Pathol. 36 (2), 277–278. https://doi.org/10.1177/0192623307313010.
Zhao, Y., Rafatian, N., Feric, N.T., Cox, B.J., Aschar-Sobbi, R., Wang, E.Y., Aggarwal, P., Zhang, B., Conant, G., Ronaldson-Bouchard, K., Pahnke, A., Protze, S., Lee, J.H., Davenport Huyer, L., Jekic, D., Wickeler, A., Naguib, H.E., Keller, G.M., Vunjak-Novakovic, G., Broeckel, U., Backx, P.H., Radisic, M., 2019. A platform for generation of chamber-specific cardiac tissues and disease modelling. Cell 176 (4). https://doi.org/10.1016/j.cell.2018.11.042, 913-927.e18.